DOI: 10.18721/JPM.10404
UDC 536.24.08

CHEMICAL REACTION AND THERMAL RADIATION EFFECTS ON A BOUNDARY LAYER FLOW OF NANOFLUID OVER A WEDGE WITH VISCOUS AND OHMIC DISSIPATION

A.K. Pandey[1,2], M. Kumar[2]

[1] Roorkee Institute of Technology, Roorkee, India;

[2] G.B. Pant University of Agriculture and Technology, Pantnagar, India

In this article, we have analyzed the influence of a chemical reaction and thermal radiation on a magnetohydrodynamic (MHD) flow of (Cu − water) nanofluid past a wedge in the occurrence of viscous and Ohmic dissipation. The nonlinearity numerical approach called the Runge − Kutta − Fehlberg method of the 4^{th}-5^{th} order was used with shooting technique to find the results of velocity, temperature and concentration fields for several points of the parameters taken. The skin friction coefficient, the Nusselt and the Sherwood numbers were examined in details and the results were presented in graphic and tabular forms. An analysis of the obtained results revealed that the concentration boundary layer thickness diminishes with an increase in the values of the chemical reaction parameter and the velocity profiles increase with increasing the magnetic field parameter.

Keywords: chemical reaction; nanofluid; Ohmic dissipation; thermal radiation; viscous dissipation

Citation: A.K. Pandey, M. Kumar, Chemical reaction and thermal radiation effects on a boundary layer flow of nanofluid over a wedge with viscous and Ohmic dissipation, St. Petersburg Polytechnical State University Journal. Physics and Mathematics. 10 (4) (2017) 54–72. DOI: 10.18721/JPM.10404

ВЛИЯНИЕ ХИМИЧЕСКОЙ РЕАКЦИИ И ТЕПЛОВОГО ИЗЛУЧЕНИЯ НА ХАРАКТЕРИСТИКИ ПОГРАНИЧНОГО СЛОЯ ПОТОКА НАНОЖИДКОСТИ, ОБТЕКАЮЩЕГО КЛИН С ВЯЗКОЙ И ОМИЧЕСКОЙ ДИССИПАЦИЯМИ

А.К. Панди[1,2], М. Кумар[2]

[1] Индийский технологический институт Рурки, г. Рурки, Индия;

[2] Университет сельского хозяйства и технологии им. Г.Б. Панта, г. Пантнагар, Индия

В статье проанализировано влияние теплового излучения и химической реакции на свойства магнитогидродинамического (МГД) потока наножидкости (наночастицы меди в воде), обтекающего твердый клин с вязкой и омической диссипациями. Для нахождения профилей скорости, температуры и концентрации наночастиц для нескольких значений заданных параметров использовано нелинейное численное приближение, называемое методом Рунге − Кутта − Фельберга 4-го и 5-го порядков с математическим пристреливанием. Значения коэффициента поверхностного трения, чисел Нуссельта и Шервуда детально изучены, и результаты представлены в виде графиков и таблиц. Анализ полученных расчетных результатов привел к заключению, что толщина концентрационного граничного слоя потока снижается с увеличением параметра реакции, а скорости потока растут с увеличением параметра магнитного поля.

Ключевые слова: химическая реакция; наножидкость; омическая диссипация; тепловое излучение; вязкая диссипация

Ссылка при цитировании: Панди А.К., Кумар М. Влияние химической реакции и теплового излучения на характеристики пограничного слоя потока наножидкости, обтекающего клин с вязкой и омической диссипациями // Научно-технические ведомости СПБГПУ. Физико-математические науки. 2017. Т. 10. № 4. С. 54–72. DOI: 10.18721/JPM.10404

1. Introduction

Due to low thermal conductivity, conventional fluids like water, ethylene glycol and oil have a restricted cooling performance. Choi [1] illustrated that this restricted cooling performance can be determined by the addition of a small amount of high-heat transfer performance of solid nanoparticles to the traditional fluid to form the so-called nanofluids. Typically, the particles in such nanofluids have dimensions ranging from 1 to 100 nm and take the form of metals, oxides, carbides, nitrides or nonmetals. There are several engineering and physical applications of heat transfer in nanofluid such as engine cooling, refrigerators, chillers, microelectronics, fuel cells, etc.

Magnetic nanofluid is a magnetic colloidal suspension of carrier liquid and magnetic nanoparticles. The assistance of magnetic nanofluid is that fluid flow and heat transfer can be managed with the aid of an external source, which makes it pertinent to several areas such as aerospace, electronic packing and thermal engineering. In other words, flow behavior is heavily affected by the intensity and orientation of the applied magnetic field. The applied magnetic field influences the suspended particles and reshuffles their concentration within the fluid, which convincingly alters the flow characteristics of heat transfer. Alternatively, the study of magnetohydrodynamic (MHD) flow for an electrically conducting fluid flow over a heated wedge surface has a lot of significant applications in engineering fields such as nuclear reactors cooling, MHD power generators, studies of plasma and petroleum engineering. Moreover, magnetohydrodynamics is also used in metallurgical processes and boundary layer flow. The effects of MHD flow past a wedge surface due to nanofluid have been analyzed in a few studies.

Ariel [2] studied the influence of the magnetic field on laminar flow of two-dimensional incompressible glutinous fluid impinging normal to the plane. The author established that with increasing values of the Hartmann number, the shear stress rate increases as well. The effect of suction/injection on a two-dimensional steady nanofluid MHD flow due to a vertical wedge in the existence of mixed convection and chemical reaction was studied by Ganapathirao et al. [3]. Rahman et al. [4] described the impact of heat generation/absorption on a two-dimensional steady nanofluid flow over a wedge with convective surface. They discovered that the Nusselt number increased with increasing values of the Biot number and slip parameter. Srinivasacharya et al. [5] have proposed the effect of heat and mass transfer rate on MHD flow over a wedge within the nanofluid. Rahman et al. [6] investigated the simultaneous impact of heat and mass transfer on an unsteady MHD flow of nanofluid over a wedge surface with thermophoresis and variable electric conductivity. Yacob et al. [7] have considered a flow of nanofluid over a stationary or a moving wedge. The impact of viscous dissipation with a slip wall on an unsteady MHD flow over a stretching wedge for nanofluid have been described by Nagendramma et al. [8]. Kandasamy et al. [9] considered the influence of thermal radiation on an unsteady MHD flow of nanofluid over a porous wedge. Recently, we [10] have analyzed the influence of suction/injection on MHD flow of nanofluid due to a porous wedge in the existence of viscous dissipation and slip. We revealed that the skin friction coefficient increases with an increase in the Eckert number. Then we [11] have illustrated the effect of natural convection and viscous dissipation on nanofluid flow due to a stretching cylinder with thermal radiation, porous medium and slip boundary conditions. Khanafer et al. [12] have examined heat transfer enhancement of nanofluid due to an enclosure using the single-phase model. Further, the single-phase model was used to determine the heat transfer rate of nanofluid due to different geometry by Buongiorno [13], Tiwari and Das [14]. Sheikholeslami and Abelman [15] examined the impact of the magnetic field on a nanofluid flow due to two coaxial cylinders

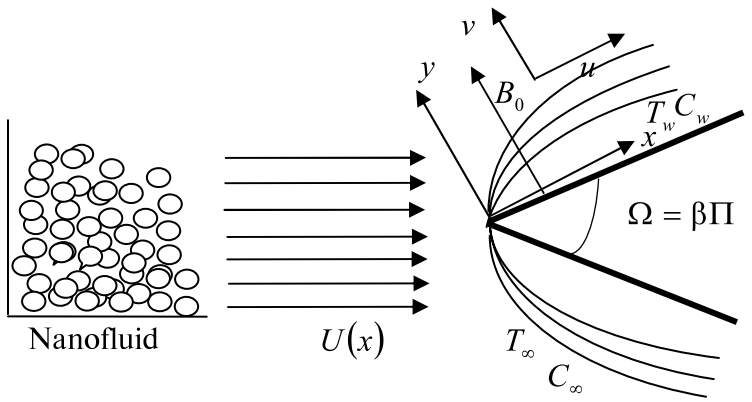

Fig. 1. Physical model of the flow over a wedge surface and the coordinate system: $U(x)$ is the uniform velocity, B_0 is the uniform magnetic field, Ω is the total wedge angle, T is the temperature, C is the specific heat

by applying the two-phase model. Again, the impact of MHD flow of nanofluid over different surfaces has been described in several studies [16 – 38]. We [39] have investigated the numerical solution of nanofluid flow past a stretching cylinder under slip conditions. Hayat et al. [40] have examined the mixed convection stagnation point flow of tangent hyperbolic nanofluid towards a stretching sheet. Mustafa et al. [41] have solved the problem of nanofluid flow within a channel with complaint walls by the Homotopy Analysis Method (HAM) and the shooting method.

Several chemically reacting systems incorporate both homogeneous and heterogeneous reactions, with instances happening in catalysis, combustion and biochemical systems. The interaction between homogeneous reactions within the bulk of the fluid and heterogeneous reactions occurring on some catalytic surfaces is usually extremely complex and is relevant in the production and consumption of reactant species at various rates both in the fluid and surfaces of catalytic. Stagnation-point boundary layer flow due to homogeneous and heterogeneous reactions was studied by Chaudhary and Merkin [42]. Similarly, several studies [43 – 50] revealed the influence of homogeneous and heterogeneous reactions on different types of fluid for different geometry.

The present work deals with the influence of viscous and Ohmic dissipation on a two-dimensional steady nanofluid MHD flow past a wedge surface in the existence of thermal radiation and chemical reaction.

To the best of our knowledge, no recent studies have been completed on this subject. The numerical solution of the recent study was acquired by applying the shooting method based on the Runge – Kutta – Fehlberg scheme. The influence of different pertinent parameters on flow field, thermal field and concentration were considered graphically and described in details. The boundary layer flow due to a wedge surface plays a key role in the field of crude oil extraction, heat exchangers, ground water pollution, geothermal systems, etc.

2. Mathematical formulation

We assume the existence of a steady flow of two-dimensional and incompressible conventional water-based nanofluid, including copper (Cu) as nanoparticles that moves over the surface of a wedge with a uniform velocity $U(x)$, and a variable magnetic field

$$B(x) = B_0 x^{\frac{(m-1)}{2}},$$

(B_0 is a magnetic field of a uniform strength); the external flow velocity has the form

$$U(x) = u_0 x^m,$$

where u_0 is a constant (see Ref. [5]), whereas

$$m = \frac{\beta}{2-\beta}$$

is the power-law Falkner – Skan parameter

$(0 \le m \le 1)$; $\beta = \Omega / \Pi$ is the pressure gradient parameter also known as the Hartree pressure gradient (Ω is the total wedge angle assuming two dissimilar values of the Hartree parameter β, i.e., with the flow past a horizontal wall $\beta = 0$ ($\Omega = 0°$) and $\beta = 1(\Omega = 180°)$ for boundary layer flow near an upright flat plate.

It is assumed that the fluid phase and the solid particles are in a thermal equilibrium state and that they flow with an equal local velocity. The geometry of the present model is shown in Fig. 1.

The conventional equations of continuity, momentum, heat transfer and concentration are expressed as [5]:

$$\frac{\partial u}{\partial x} + \frac{\partial v}{\partial y} = 0; \tag{1}$$

$$u\frac{\partial u}{\partial x} + v\frac{\partial u}{\partial y} = U\frac{dU}{dx} + \frac{\mu_{nf}}{\rho_{nf}}\frac{\partial^2 u}{\partial y^2} + \frac{\sigma B^2}{\rho_{nf}}(U-u); \tag{2}$$

$$u\frac{\partial T}{\partial x} + v\frac{\partial T}{\partial y} = \alpha_{nf}\frac{\partial^2 T}{\partial y^2} + \frac{\mu_{nf}}{(\rho C_p)_{nf}}\left(\frac{\partial u}{\partial y}\right)^2 + \frac{\sigma B^2}{(\rho C_p)_{nf}}u^2 - \frac{1}{(\rho C_p)_{nf}}\frac{\partial q_r}{\partial y}; \tag{3}$$

$$u\frac{\partial C}{\partial x} + v\frac{\partial C}{\partial y} = D\frac{\partial^2 C}{\partial y^2} - K_1(C - C_\infty). \tag{4}$$

The boundary conditions are as follows:

$$\left.\begin{aligned} &u = 0,\ v = 0,\ T = T_w,\ C = C_w \text{ as } y \to 0;\\ &u = u_0 x^m,\ T = T_\infty,\ C = C_\infty \text{ at } y \to \infty, \end{aligned}\right\} \tag{5}$$

where (u, v) are the velocity components along the x and y axes, respectively.

The effective dynamic viscosity μ_{nf}, the effective density ρ_{nf}, the thermal diffusivity α_{nf}, the heat capacitance $(\rho C_p)_{nf}$ and the thermal conductivity k_{nf} of the nanofluid are defined as [4, 7, 10]:

$$\left.\begin{aligned} &\mu_{nf} = \frac{\mu_f}{(1-\phi)^{2,5}},\\ &\rho_{nf} = (1-\phi)\rho_f + \phi\rho_s,\ \alpha_{nf} = \frac{k_{nf}}{(\rho C_p)_{nf}};\\ &(\rho C_p)_{nf} = (1-\phi)(\rho C_p)_f + \phi(\rho C_p)_s,\\ &\frac{k_{nf}}{k_f} = \frac{k_s + 2k_f - 2\phi(k_f - k_s)}{k_s + 2k_f + \phi(k_f - k_s)}. \end{aligned}\right\} \tag{6}$$

where ϕ is the volume fraction of the solid and the subscripts f and s denote the fluid and the solid nanoparticles, respectively. The thermophysical properties of the nanofluid are listed in Table 1.

With the help of the Rosseland approximation, the radiation heat flux is defined as [9]:

$$q_r = -\frac{4\sigma^*}{3k^*}\frac{\partial T^4}{\partial y} \tag{7}$$

where σ^* and k^* are the Stefan – Boltzmann constant and the coefficient of mean absorption; T^4 is the linear sum of temperature and it can be expanded with the help of the Taylor series along with T_∞ :

$$T^4 = T_\infty^4 + 4T_\infty^3(T - T_\infty) + 6T_\infty^2(T - T_\infty)^2 + \ldots . \tag{8}$$

Vanishing the higher terms of $(T - T_\infty)$ in Eq. (8), we obtain

$$T^4 \cong 4T_\infty^3 T - 3T_\infty^4. \tag{9}$$

Solving Eqs. (7) and (9) we get

$$q_r = -\frac{16T_\infty^3\sigma^*}{3k^*}\frac{\partial T}{\partial y}. \tag{10}$$

The following nondimensional similarity transformations are introduced [5]:

$$\psi = (\nu_f x^{m+1})^{1/2} f(\eta),\ \ \eta = \left(\frac{u_0 x^{m+1}}{\nu_f}\right)\frac{y}{x}, \tag{11}$$

Table 1

Thermophysical properties of water and nanoparticles [4, 7]

Substance	ρ, kg/m^3	C_p, J/(kg·K)	k, W/(m·K)
Pure water	997.1	4179	0.613
Copper (Cu)	8933	385	400

Notations: ρ is the density, C_p is the specific heat at the constant pressure, k is the thermal conductivity coefficient.

$$\theta(\eta) = \frac{T - T_\infty}{T_W - T_\infty}, \quad T_W - T_\infty = x\Delta T,$$
$$\chi(\eta) = \frac{C - C_\infty}{C_W - C_\infty}, \quad C_W - C_\infty = x\Delta C, \tag{11}$$

where $\psi(x, y)$ is the stream function written as

$$u = \frac{\partial\psi}{\partial y}, \quad v = -\frac{\partial\psi}{\partial x}; \tag{12}$$
$$u = u_0 x^m f',$$

$$v = -\frac{1}{2}(m+1)(\nu_f u_0 x^{m-1})^{\frac{1}{2}} \times \left[f + \left(\frac{m-1}{m+1}\right)\eta f' \right]. \tag{13}$$

Now let us substitute Eqs. (6), (10) – (13) into Eqs. (2), (3) and (4), respectively. The following nonlinear ordinary difference equations (ODEs) of momentum, energy and mass transfer are obtained:

$$f''' - \phi_1 \left[m f'^2 - \left(\frac{m+1}{2}\right) f f'' - m \right] + (1-\phi)^{2,5} M(1 - f') = 0, \tag{14}$$

$$(1+R)\theta'' + \Pr \frac{k_f}{k_{nf}} \phi_2 \left(\frac{m+1}{2} f\theta' - f'\theta \right) + Ecf''^2 + M\mathrm{Ec}(1-\phi)^{2,5} f'^2 = 0, \tag{15}$$

$$\chi'' + \mathrm{Sc}\left(\frac{m+1}{2} f\chi' - (f' + \gamma)\chi \right) = 0, \tag{16}$$

and boundary conditions (5) turn into the following ones:

$$\left.\begin{array}{l} f'(0) = 0,\ f(0) = 0, \theta(0) = 1, \\ \chi(0) = 1 \text{ at } \eta = 0; \\ f' = 1,\ \theta = 0,\ \chi = 0 \text{ as } \eta \to \infty, \end{array}\right\} \tag{17}$$

where the prime indicates the derivative with respect to η; the dimensionless parameters are $\Pr$, the Prandtl number; Sc, the Schmidt number; M, the magnetic field parameter; Ec, the Eckert number; R, the radiation parameter; γ, the chemical reaction parameter; ϕ_1, ϕ_2, the constants, respectively, defined as:

$$\Pr = \frac{\nu_f (\rho C_p)_f}{k_f}, \ \mathrm{Sc} = \frac{\nu_f}{D}, \ M = \frac{\sigma B_0^2}{\rho_f u_0}, \tag{18}$$

$$\mathrm{Ec} = \frac{\mu_{nf} U^2}{k_{nf}(T_W - T_\infty)}, \quad R = \frac{16\sigma^* T_\infty^3}{3k^* k_{nf}},$$
$$\gamma = \frac{U(x)K_1}{x},$$
$$\phi_1 = (1-\phi)^{2,5}\left[1 - \phi + \phi\frac{\rho_s}{\rho_f}\right],$$
$$\phi_2 = 1 - \phi + \phi\frac{(\rho C_p)_s}{(\rho C_p)_f}. \tag{18}$$

For practical interest, the shear stress rate (the skin friction coefficient C_f), heat transfer rate (the Nusselt number Nu_x) and mass transfer rate (the Sherwood number Sh_x) are expressed as:

$$C_f = \frac{\mu_{nf}}{\rho U^2}\left(\frac{\partial u}{\partial y}\right)_{y=0},$$
$$\mathrm{Nu}_x = \left(\frac{kx}{k_f (T_w - T_\infty)}\right)\left(\frac{\partial T}{\partial y}\right)_{y=0}, \tag{19}$$
$$\mathrm{Sh}_x = \frac{x}{(C_w - C_\infty)}\left(\frac{\partial C}{\partial y}\right)_{y=0}.$$

Hence, the reduced dimensionless skin friction coefficient, the heat transfer coefficient and the reduced mass transfer coefficient are defined as:

$$(1-\phi)^{2,5}\sqrt{\mathrm{Re}_x} C_f = 2f''(0),$$
$$\frac{\mathrm{Nu}_x}{\sqrt{\mathrm{Re}_x}}\frac{k_f}{k_{nf}} = -(1+R)\theta'(0), \tag{20}$$
$$\frac{\mathrm{Sh}_x}{\sqrt{\mathrm{Re}_x}}\frac{k_f}{k_{nf}} = -\chi'(0)$$

where $\mathrm{Re}_x = xU/\nu_f$ is the local Reynolds number.

3. Numerical method

The nondimensional momentum (Eq. (14)), energy (Eq. (15)) and concentration (Eq. (16)) together with supporting boundary conditions (17) have been dealt with numerical solution by applying the shooting procedure with the $4^{\text{th}} - 5^{\text{th}}$ order Runge – Kutta – Fehlberg (RKF) integration formula. For this scheme, we first modify the primary differential equations into

a set of the first order ODEs.

Let us presume that

$$y_1 = \eta,\ \ y_2 = f,\ \ y_3 = f',\ \ y_4 = f'',$$
$$y_5 = \theta,\ \ y_6 = \theta',\ \ y_7 = \chi,\ \ y_8 = \chi'.$$

Now we obtain a first-order system of Eqs.:

$$\begin{pmatrix} y_1' \\ y_2' \\ y_3' \\ y_4' \\ y_5' \\ y_6' \\ y_7' \\ y_8' \end{pmatrix} = \tag{21}$$

$$= \begin{pmatrix} 1 \\ y_3 \\ y_4 \\ \phi_1\left(my_3^2 - \left(\frac{m+1}{2}\right)y_2y_4 - m\right) - \\ -(1-\phi)^{2,5}M(1-y_3) \\ y_6 \\ \frac{-1}{(1+R)}\left(\phi_2\,\mathrm{Pr}\,\frac{k_f}{k_{nf}}\left(\frac{m+1}{2}y_2y_6 - y_3y_5\right) + \right. \\ \left. + \ \mathrm{Ec}y_4^2 + (1-\phi)^{2,5}M\mathrm{Ec}y_3^2\right) \\ y_8 \\ -\mathrm{Sc}\left(\frac{m+1}{2}y_2y_8 - y_7(y_3+\gamma)\right) \end{pmatrix}.$$

The associated initial conditions are:

$$\begin{pmatrix} y_1 \\ y_2 \\ y_3 \\ y_4 \\ y_5 \\ y_6 \\ y_7 \\ y_8 \end{pmatrix} = \begin{pmatrix} 0 \\ 0 \\ 0 \\ q_1 \\ 1 \\ q_2 \\ 1 \\ q_3 \end{pmatrix}. \tag{22}$$

The system of first-order ODEs (21) via initial conditions (22) is solved using a $4^{th} - 5^{th}$ order RKF integration process, and the appropriate values of unknown initial conditions q_1, q_2 and q_3 are selected and then numerical integration is applied.

Here we contrast the computed values of f', θ and χ as $\eta \to \infty$, through the specified boundary conditions

$$f'(\infty) = 1,\ \ \theta(\infty) = 0,\ \ \chi(\infty) = 0,$$

and regulate the estimated values of q_1, q_2 and q_3 to gain an excellent approximation for the result. The unknown q_1, q_2 and q_3 were approximated by Newton's scheme in such a way that boundary conditions were obeyed at highest numerical values of $\eta \to \infty$, with an error less than 10^{-8}.

4. Validation of the code

To check the accuracy of our present code, we compared the obtained results of the skin friction coefficient $(f''(0))$, for several values of the magnetic field parameter M, in the absence of thermal radiation, the viscous and Ohmic dissipation and the chemical reaction parameter for the base fluid (water) with the data obtained by Ariel [2] and Srinivasacharya et al. [5]. Notice that our results are in better agreement, as shown in Table 2. Therefore, using our recent code is valid for computation.

5. Results and discussion

The solutions of the nondimensional velocity field $f'(\eta)$, the temperature field $\theta(\eta)$, the concentration $\chi(\eta)$, the skin factor C_f, the Nusselt number Nu_x, and the Sherwood number Sh_x profiles were obtained for several values of related parameters, throughout the procedure with the step length $\Delta\eta = 0.001$, where $0 \le \eta \le 3$. Notice that for the base fluid $(\phi = 0)$, the value of the constants ϕ_1 and ϕ_2 becomes unity. The present model will be the same as the one presented by Srinivasacharya et al. [5] in the absence of viscous and Ohmic dissipation, thermal radiation and chemical reaction.

The changes in the dimensionless parameters such as the skin friction, the Nusselt number and the Sherwood number are presented in Table 3. This data reveals that the skin friction coefficient and the mass transfer rate of the

Table 2

Comparison of the values of the skin friction coefficient $f''(0)$ for different values of the magnetic field parameter M

M	$f''(0)$		
	Ariel [2]	Srinivasacharya et al. [5]	Present study
0	1.232588	1.2325965196	1.2328130
1	1.585331	1.5852800424	1.5853650
4	2.346663	2.3468696599	2.3466556
25	5.147965	5.1479646032	5.1479628
100	10.074741	10.0747411168	10.0747412

The data is given in the absence of thermal radiation, the viscous and Ohmic dissipation and the chemical reaction parameter, whereas $\phi = 0$, Ec = 0, $m = 1$, Pr = 1, $R = 0$, Sc = 0.24 and $\gamma = 0$.

Table 3

Values of the skin friction coefficient, the Nusselt number and the Sherwood number for different values of the magnetic field parameter M

M	$f''(0)$	$-\theta'(0)$	$-\chi'(0)$
0.2	1.499681	0.600960	0.680420
0.6	1.598197	0.592030	0.683610
1.0	1.691074	0.582014	0.686460
2.0	1.903826	0.553324	0.692502
3.0	2.095334	0.520750	0.697402

Notations: $f''(0)$ is the skin friction coefficient, $-\theta'(0)$ is the Nusselt number, $\chi'(0)$ is the Sherwood number.
Fixed parameter values: Ec = 0.1, $m = 1$, Pr = 1, $R = 0.5$, Sc = 0.24, $\phi = 0.1$, $\gamma = 1$.

Cu–water nanofluid increase with increasing the magnetic field parameter M. Moreover, the heat transfer rate decelerates with an increase in M.

Table 4 indicates that the Sherwood number depends on the chemical reaction parameter γ. We can see that the mass transfer rate of nanofluid accelerates with increasing γ. The

Table 4

Values of the Sherwood number for different values of the chemical reaction parameter γ

γ	$-\chi'(0)$
0	0.518711
5	1.165433
20	2.213661
40	3.110745
50	3.474195
60	3.803274

Fixed parameter values: Ec = 0.1, $M = 0.6$, $m = 1$, Pr = 1, $R = 0.5$, Sc = 0.24, $\phi = 0.1$.

Table 5

Values of the Nusselt number for different values of the radiation parameter R

R	$-\theta'(0)$
0	0.454424
1	0.421124
4	0.378224
12	0.352560
20	0.345560

Fixed parameter values: $\gamma = 1$, Ec = 0.1, $M = 0.6$, $m = 1$, Pr = 1, Sc = 0.24, $\phi = 0.1$.

heat transfer coefficient in terms of the Nusselt number is given in Table 5 for different values of R. This data signifies that the heat transfer rate decelerates with increasing R. The influence of the related parameters on the velocity, temperature and volume concentration of nanoparticles is illustrated in Figs. 2 – 5. In the recent study we have regarded Cu (copper) as nanoparticles and water as a base fluid. The impact of the magnetic parameter M on the flow field, thermal field and concentration of Cu–water nanofluid for $\mathrm{Pr} = m = 1$, $\mathrm{Ec} = \phi = 0.1$, $R = 0.5$, $\gamma = 1$ and $\mathrm{Sc} = 0.24$ are shown in Fig. 2. Fig. 2, *a* shows that the velocity field profile of the Cu–water nanofluid increases with increasing the magnetic parameter and it is also obvious from this graph that the momentum boundary layer width of the nanofluid decreases. We used Fig. 2, *b* to conclude that the thermal field component is influenced by the magnetic field parameter M in the domain of [0, 3] and the trend of the

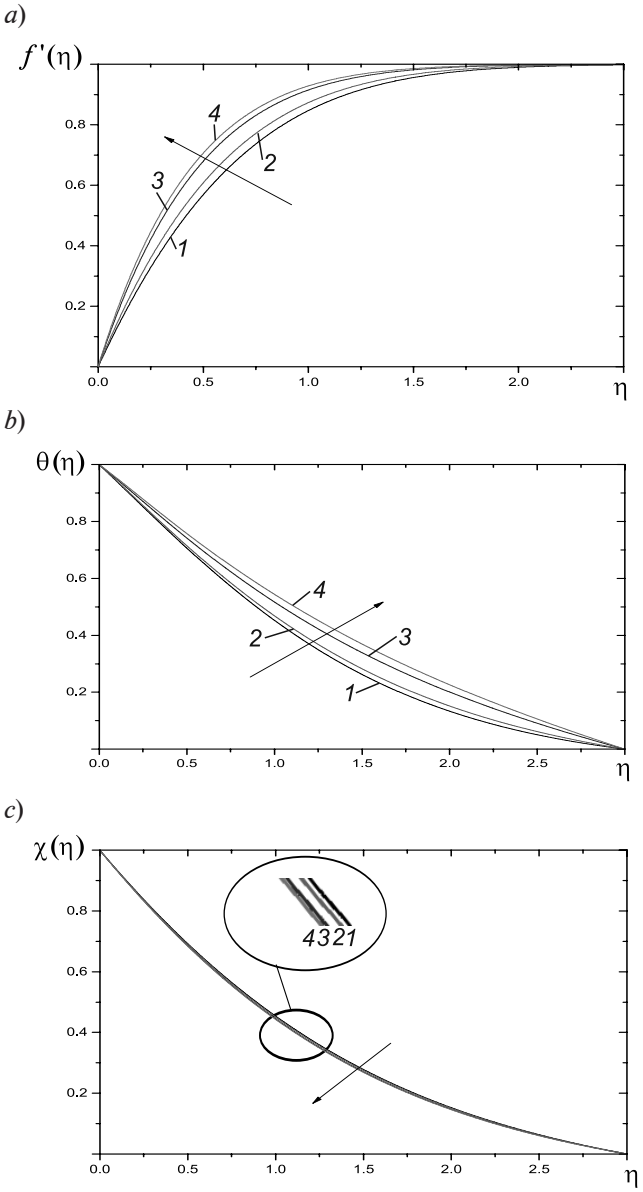

Fig. 2. Velocity (*a*), temperature (*b*) and concentration (*c*) profiles of Cu–water nanofluid for different values of the magnetic field parameter M: 0.2 (*1*), 1.0 (*2*), 3.0 (*3*), 4.0 (*4*); $\mathrm{Pr} = m = 1$, $\mathrm{Ec} = \phi = 0.1$, $R = 0.5$, $\gamma = 1$, $\mathrm{Sc} = 0.24$

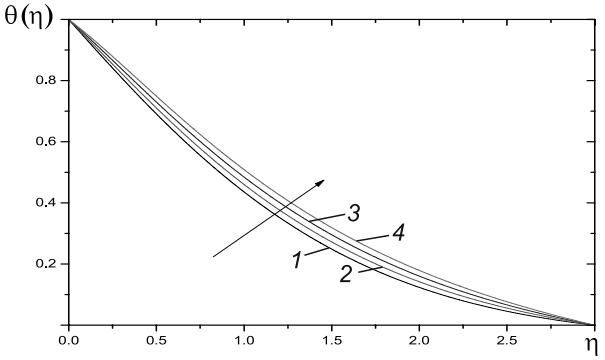

Fig. 3. Temperature profiles of Cu–water nanofluid for different values of the Eckert number Ec: 0(*1*), 0.1 (*2*), 0.2 (*3*), 0.3 (*4*); $M = 0.6$, $\mathrm{Pr} = m = \gamma = 1$, $R = 0.5$, $\phi = 0.1$

dimensionless temperature profiles increases with increasing M in this entire domain. For this reason, the thermal boundary layer thickness grows to large values. Similarly, we can see from Fig. 2, *c* that the concentration graph varies with the magnetic parameter corresponding to each value of the horizontal component η.

In the regions of [0, 0.2] and [2.9, 3.0], there is no change in the concentration profile of the Cu–water nanofluid; the fluid concentration subsequently decreases with increasing the values of M in the region of [0.2, 2.9].

The deviation in the temperature distribution corresponding to the horizontal variable η

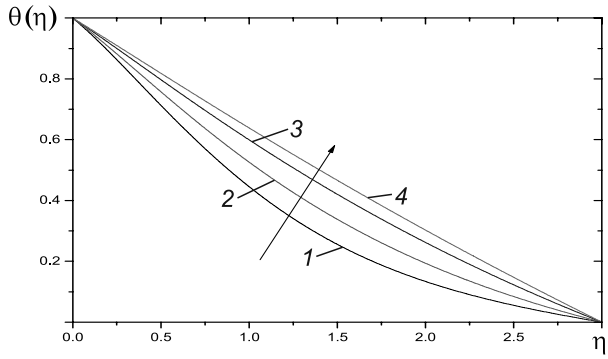

Fig. 4. Temperature profiles of Cu–water nanofluid for different values of the radiation parameter R: 0 (*1*), 1 (*2*), 4 (*3*), 12 (*4*); $M = 0.6$, $\mathrm{Pr} = m = \gamma = 1$, $\mathrm{Ec} = 0.3$, $\phi = 0.1$

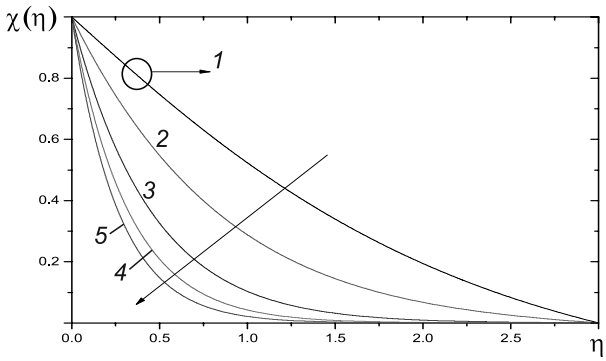

Fig. 5. Concentration profiles of Cu–water nanofluid for different values of the chemical reaction parameter γ: 0(*1*), 5(*2*), 20(*3*), 40(*4*), 60(*5*); $M = 0.6$, $\mathrm{Pr} = m = 1$, $R = 0.5$, $\mathrm{Ec} = \phi = 0.1$

for different values of the Eckert number Ec is shown in Fig. 3 for $M = 0.6$, $\mathrm{Pr} = m = \gamma = 1$, $R = 0.5$ and $\phi = 0.1$.

We can conclude from this figure that the temperature of the nanoparticles gradually increases with increasing the values of the Eckert number, and for this reason the width of the thermal boundary layer increases. Moreover, the heat transfer rate decreases for different values of the Eckert number Ec.

The graph for the thermal field versus the horizontal axis η for different values of the radiation parameter R with $M = 0.6$, $\mathrm{Pr} = m = \gamma = 1$, $\mathrm{Ec} = 0.3$ and $\phi = 0.1$ is shown in Fig. 4. It is clear from this figure that the temperature of the nanoparticle increases with increasing thermal radiation parameter, while the heat transfer rate decreases with increasing the R value.

Fig. 5 shows the graph for the concentra-

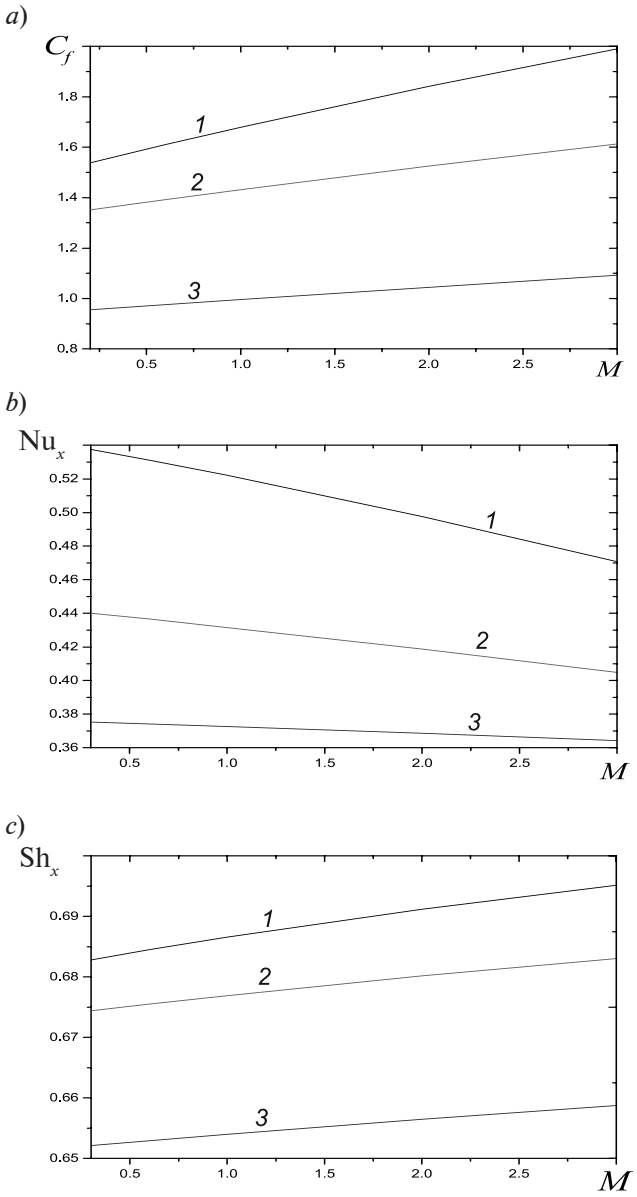

Fig. 6. The plots of the skin friction coefficient (*a*), the Nusselt (*b*) and the Sherwood (*c*) numbers versus M parameter for different values of the solid volume fraction ϕ: 0.2 (*1*), 0.4 (*2*), 0.6 (*3*); $\mathrm{Pr} = m = \gamma = 1$, $R = 0.5$, $\mathrm{Ec} = 0.1$, $\mathrm{Sc} = 0.24$

tion profile of the Cu–water nanofluid versus variable η, for different values of the chemical reaction parameter γ at $M = 0.6$, $\mathrm{Pr} = m = 1$, $R = 0.5$ and $\mathrm{Ec} = \phi = 0.1$. It can be seen that this concentration profile of the Cu–water nanofluid asymptotically approaches zero in the region of $[0, \infty)$. In other words, it decreases gradually with increasing the chemical reaction parameter γ in the dynamic range of $0 \le \eta < \infty$; moreover, the curve is asymptotic to the axis of η; we can also conclude that the concentration boundary layer thickness decreases gradually. However, the mass transfer rate increases monotonically.

The changes in the nondimensional skin friction coefficient, the Nusselt number and the Sherwood number depending on the magnetic field parameter M for different values of the solid volume fraction ϕ are shown in Fig. 6 with the parameter values $\mathrm{Pr} = m = \gamma = 1$, $R = 0.5$, $\mathrm{Ec} = 0.1$ and $\mathrm{Sc} = 0.24$. The influence of the volume fraction ϕ on the skin friction coefficient is demonstrated in Fig. 6, *a*. It can be seen from this graph that each value of the thermal radiation skin friction decreases with increasing the volume concentration of solid particles. The graph of the Nusselt number versus the magnetic field parameter for several values of the solid concentration is shown in Fig. 6, *b*. It can be seen that the heat transfer rate increases with increasing the concentration of solid particles.

The variation in the mass transfer rate with respect to the variable M for different values of the volume concentration is shown in Fig. 6, *c*. It can be seen that the Sherwood number is an increasing function of ϕ in the domain M.

The effect of the volume concentration along with the thermal radiation parameter R on the Nusselt number is shown in Fig. 7, with the values of nondimensional parameters $\mathrm{Pr} = m = \gamma = 1$, $M = 0.6$, $\mathrm{Ec} = 0.3$ and $\mathrm{Sc} = 0.24$. This figure shows that the heat transfer rate enhances with the solid volume concentration for each value of the radiation parameter.

Fig. 8 shows the changes in velocity, temperature and concentration profiles of the nanofluid for different values of m with $\mathrm{Ec} = 0.3$, $M = 0.6$, $\mathrm{Pr} = 1$, $R = \gamma = 1$, $\mathrm{Sc} = 0.94$ and $\phi = 0.6$. Fig. 8, *a* shows that the velocity profiles frequently increase with increasing the values of m in the region of [0, 3]. Fig. 8, *b* shows that the temperature profiles decrease with increasing m within the domain of (0.5, 0.9). Similarly, it can be seen from Fig. 8, *c* that the concentration profiles of the nanofluid gradually decreased with increasing m in the specified range, and for this reason, the concentration boundary layer thickness decreased.

The influence of the Prandtl number with $\mathrm{Ec} = 0.3$, $M = 0.6$, $m = 1$, $R = \gamma = 1$, $\mathrm{Sc} = 0.94$ and $\phi = 0.6$ on the temperature distribution is shown in Fig. 9. We can see from these curves that the temperature profiles gradually decrease with increasing the Prandtl number. Fig. 10 shows the effect of the Schmidt number Sc on

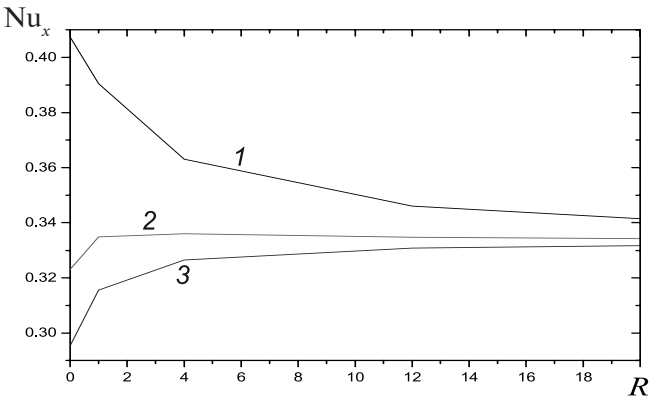

Fig. 7. The plots of the Nusselt number versus R parameter for different values of the solid volume fraction ϕ: 0.2 (*1*), 0.4 (*2*), 0.6 (*3*); $\mathrm{Pr} = m = \gamma = 1$, $M = 0.6$, $\mathrm{Ec} = 0.3$, $\mathrm{Sc} = 0.24$

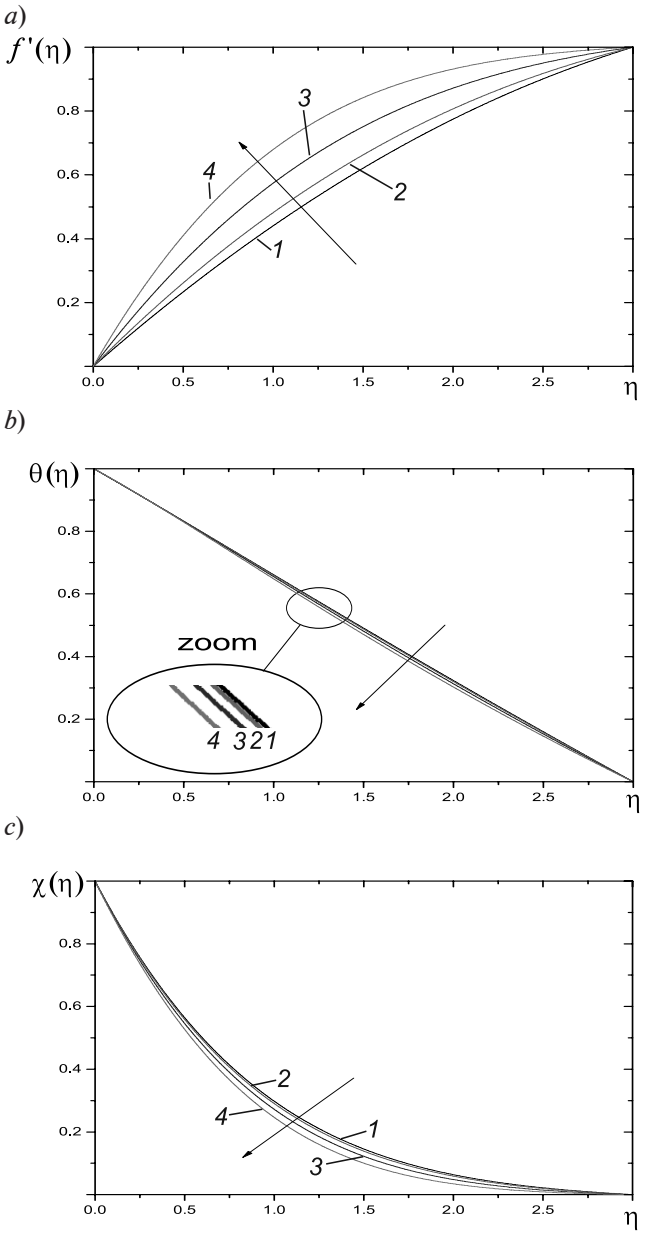

Fig. 8. Velocity (*a*), temperature (*b*) and concentration (*c*) profiles of the nanofluid for different values of the power-law Falkner – Skan parameter *m*: 1/11 (*1*), 0.2 (*2*), 0.5 (*3*), 1.0 (*4*);
Ec = 0.3, $M = 0.6$, Pr = 1, $R = \gamma = 1$, Sc = 0.94, $\phi = 0.6$

the concentration distribution of the nanofluid with Ec = 0.3, $M = 0.6$, $m = 1$, $R = \gamma = 1$, Pr = 1 and $\phi = 0.6$. It can be seen from these curves that the concentration profiles increase with increasing the Schmidt number, and for this reason the solution boundary layer thickness decreases with increasing the Sc value.

Table 6 shows the values of the skin friction coefficient, the Nusselt and the Sherwood numbers due to the effect of *m*. It can be seen from this data that the mass transfer rate and the shear stress rate increase with increasing *m*, while the heat transfer rate decreases.

The effects of the Prandtl number on the Nusselt number are described in Table 7. We can conclude from the data that the heat

transfer rate increases along with the Prandtl number.

Table 8 describes the effect of the Schmidt number Sc on the mass transfer rate, which proves that the mass transfer rate is an increasing function of Sc.

The combined effect of the magnetic parameter M and the volume fraction ϕ of nanoparticles on the heat and mass transfer is illustrated in Table 9. It can be seen from the table that the heat transfer rate decreases but the mass transfer rate increases with increasing M for each ϕ value.

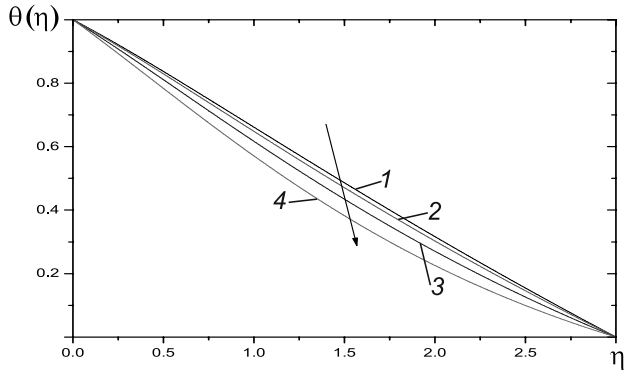

Fig. 9. Temperature profiles for different values of the Prandtl number (Pr): 0.71 (*1*), 1.00 (*2*), 1,74 (*3*), 2.97 (*4*);
Ec = 0.3, M = 0.6, m = 1, $R = \gamma$ = 1, Sc = 0.94, ϕ = 0.6

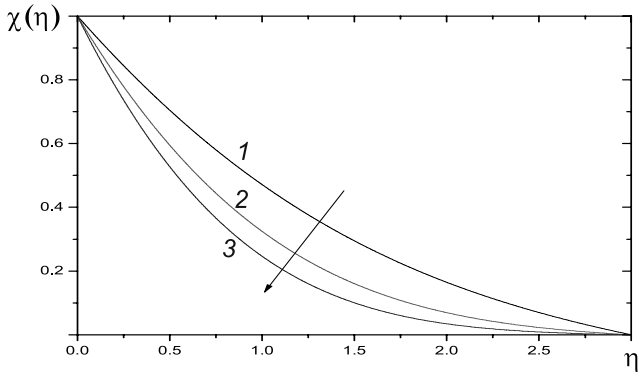

Fig. 10. Concentration profiles for different values of the Schmidt number (Sc): 0.24 (*1*), 0.60 (*2*), 0.94 (*3*);
Ec = 0.3, M = 0.6, m = 1, $R = \gamma$ = 1, Pr = 1, ϕ = 0.6

Table 6

Values of the skin friction coefficient, the Nusselt number and the Sherwood number for different values of *m*

m	$f''(0)$	$-\theta'(0)$	$-\chi'(0)$
1/11	0.4942973	0.328434	1.083905
0.2	0.5661611	0.327020	1.096231
0.5	0.7403936	0.322560	1.126572
1.0	0.9757923	0.315531	1.169118

Fixed parameter values: Ec = 0.3, M = 0.6, Pr = 1, $R = \gamma$ = 1, Sc = 0.94, ϕ = 0.6

Table 7

Values of the Nusselt number for different values of the Prandtl number

Pr	$-\theta'(0)$
0.71	0.299350
1.00	0.315531
1.74	0.354443
2.97	0.412683

Fixed parameter values: Ec = 0.3, M = 0.6, $R = m = \gamma = 1$, Sc = 0.94, ϕ = 0.6

Table 8

Values of the Sherwood number for different values of the Schmidt number Sc

Sc	$-\chi'(0)$
0.24	0.6529234
0.60	0.9583910
0.94	1.1694180

Fixed parameter values: Ec = 0.3, M = 0.6, Pr = $R = m = \gamma = 1$, ϕ = 0.6

Table 9

Effect of M and ϕ parameters on the Nusselt and the Sherwood numbers

M	$-\theta'(0)$			$-\chi'(0)$		
	$\phi = 0.2$	$\phi = 0.4$	$\phi = 0.6$	$\phi = 0.2$	$\phi = 0.4$	$\phi = 0.6$
0.2	0.539740	0.441265	0.37563	0.682209	0.674028	0.65184
0.6	0.531212	0.436532	0.37416	0.684490	0.675504	0.65292
1.0	0.522150	0.431630	0.37264	0.686579	0.676920	0.65397
2.0	0.497546	0.418689	0.36861	0.691196	0.680160	0.65645
5.0	0.470718	0.404920	0.36433	0.695133	0.683067	0.65875

Fixed parameter values: Pr = $m = \gamma = 1$, R = 0.5, Ec = 0.1, Sc = 0.24

6. Conclusions

In the current study, the effect of viscous and Ohmic dissipation on magnetohydrodynamic flow of nanofluid (Cu − water) past a wedge in the existence of thermal radiation and chemical reaction has been studied. The governing PDEs were transformed into a set of ODEs by employing the corresponding similarity transformations and the transformed equations were solved along with the boundary conditions by the Runge − Kutta − Fehlberg method of the 4^{th}-5^{th} order via the shooting technique.

The following major conclusions can be drawn from the results of our study:

The velocity of the (Cu−water) nanofluid flow increases with increasing the magnetic field parameter;

The thermal boundary layer thickness increases with increasing the magnetic field parameter;

The concentration boundary layer thickness decreases with increasing the chemical reaction parameter;

The temperature profiles of the nanoparticles increase with increasing the Eckert number;

The heat transfer rate decreases with increasing the values of the thermal radiation parameter;

The mass transfer rate increases with increasing chemical reaction parameter;

The skin friction coefficient decreases with increasing the solid volume fraction and the magnetic parameter. Moreover, the opposite behaviour was observed for the Nusselt number and the Sherwood number;

The heat transfer rate increases with increasing the volume fraction, along with the radiation parameter.

Acknowledgements

The authors wish to convey their genuine gratitude to the reviewers for their essential suggestions and comments that helped to improve this manuscript. This study did not receive any specific grant from funding agencies in the public, commercial, or *n*-profit sectors.

REFERENCES

[1] **S.U.S Choi,** Enhancing thermal conductivity of fluids with nanoparticles, ASME-Publications-Fed. 231 (1995) 99–106.

[2] **P.D. Ariel,** Hiemenz flow in hydromagnetics, Acta Mech. 103 (1–4) (1994) 31–43.

[3] **M. Ganapathirao, R. Ravindran,** Nonuniform slot suction/injection into mixed convective MHD flow over a vertical wedge with chemical reaction, Procedia Eng. 127 (2015) 1102–1109.

[4] **M.M. Rahman, M.A. Al-Lawatia, I.A. Eltayeb, N. Al-Salti,** Hydromagnetic slip flow of water based nanofluids past a wedge with convective surface in the presence of heat generation (or) absorption, Int. J. Therm. Sci. 57 (2012) 172–182.

[5] **D. Srinivasacharya, U. Mendu, K. Venumadhav,** MHD boundary layer flow of a nanofluid past a wedge, Procedia Eng. 127 (2015) 1064–1070.

[6] **A.M. Rahman, M.S. Alam, M.A. Alim, M.K. Chowdhury,** Unsteady MHD forced convective heat and mass transfer flow along a wedge with variable electric conductivity and thermophoresis, Procedia Eng. 56 (2013) 531–537.

[7] **N.A. Yacob, A. Ishak, I. Pop,** Falkner–Skan problem for a static or moving wedge in nanofluids, Int. J. Therm. Sci. 50 (2) (2011) 133–139.

[8] **V. Nagendramma, K. Sreelakshmi, G. Sarojamma,** MHD heat and mass transfer flow over a stretching wedge with convective boundary condition and thermophoresis, Procedia Eng. 127 (2015) 963–969.

[9] **R. Kandasamy, I. Muhaimin, A.K. Rosmila,** The performance evaluation of unsteady MHD non-Darcy nanofluid flow over a porous wedge due to renewable (solar) energy, Renew. Energy. 64 (2014) 1–9.

[10] **A.K. Pandey, M. Kumar,** Effect of viscous dissipation and suction/injection on MHD nanofluid flow over a wedge with porous medium and slip, Alexandria Eng. J. 55 (4) (2016) 3115–3123.

[11] **A.K. Pandey, M. Kumar,** Natural convection and thermal radiation influence on nanofluid flow over a stretching cylinder in a porous medium with viscous dissipation, Alexandria Eng. J. 56 (1) (2017) 55–62.

[12] **K. Khanafer, K. Vafai, M. Lightstone,** Buoyancy-driven heat transfer enhancement in a two-dimensional enclosure utilizing nanofluids, Int. J. Heat Mass Transf. 46 (19) (2003) 3639–3653.

[13] **J. Buongiorno,** Convective transport in nanofluids, ASME J. Heat Transf. 128 (3) (2006) 240–250.

[14] **R.K. Tiwari, M.K. Das,** Heat transfer augmentation in two-sided lid-driven differentially heated square cavity utilizing nanofluids, Int. J. Heat Mass Transf. 50 (9) (2007) 2002–2018.

[15] **M. Sheikholeslami, S. Abelman,** Two-phase simulation of nanofluid flow and heat transfer in an annulus in the presence of an axial magnetic field, IEEE Trans. Nanot. 14 (3) (2015) 561–569.

[16] **M. Sheikholeslami, D.D. Ganji, M.M. Rashidi,** Magnetic field effect on unsteady nanofluid flow and heat transfer using Buongiorno model, J. Magn. Magn. Mater. 416 (2016) 164–173.

[17] **T. Hayat, M. Waqas, S.A. Shehzad, A. Alsaedi,** A model of solar radiation and Joule heating in magnetohydrodynamic (MHD) convective flow of thixotropic nanofluid, J. Mol. Liq. 215 (2016) 704–710.

[18] **M. Ziaei-Rad, M. Saeedan, E. Afshari,** Simulation and prediction of MHD dissipative nanofluid flow on a permeable stretching surface using artificial neural network, Appl. Therm. Eng. 99 (2016) 373–382.

[19] **M. Sheikholeslami, T. Hayat, A. Alsaedi,** MHD free convection of Al_2O_3–water nanofluid considering thermal radiation: a numerical study, Int. J. Heat Mass Transf. 96 (2016) 513–524.

[20] **C. Zhang, L. Zheng, X. Zhang, G. Chen,** MHD flow and radiation heat transfer of nanofluids in porous media with variable surface heat flux and chemical reaction, Appl. Math. Modell. 39(1) (2015) 165–181.

[21] **K. Das, P.R. Duari, P.K. Kundu,** Numerical simulation of nanofluid flow with convective boundary condition, J. Egypt. Math. Soc. 23(2) (2015) 435–439.

[22] **D. Pal, G. Mandal,** Hydromagnetic convective-radiative boundary layer flow of nanofluids induced by a nonlinear vertical stretching /shrinking sheet with viscous–Ohmic dissipation, Powder Technol. 279 (2015) 61–74.

[23] **T. Hayat, M.B. Ashraf, S.A. Shehzad, A. Alsaedi,** Mixed convection flow of Casson nanofluid over a stretching sheet with convectively heated chemical reaction and heat source/sink, J. Appl. Fluid Mech. 8 (4) (2015) 803–813.

[24] **T. Hayat, M.I. Khan, M. Waqas, T. Yasmeen, A. Alsaedi,** Viscous dissipation effect in flow of magnetonanofluid with variable properties, J. Mol. Liq. 222 (2016) 47–54.

[25] **T. Hayat, M.I. Khan, M. Waqas, A. Alsaedi, T. Yasmeen,** Diffusion of chemically reactive species in third grade flow over an exponentially stretching sheet considering magnetic field effects, Chinese J. Chem. Eng. 25 (3) (2016) 257–263.

[26] **H. Upreti, A.K. Pandey, M. Kumar,** MHD flow of Ag–water nanofluid over a flat porous plate

with viscous–Ohmic dissipation, suction/injection and heat generation/absorption, Alexandria Eng. J. (2017) (in press) https://doi.org/10.1016/j.aej.2017.03.018.

[27] **T. Hayat, A. Shafiq, M. Imtiaz, A. Alsaedi,** Impact of melting phenomenon in the Falkner–Skan wedge flow of second grade nanofluid: A revised model, J. Molec. Liq. 215 (2016) 664–670.

[28] **T. Hayat, S. Qayyum, M. Imtiaz, A. Alsaedi,** Comparative study of silver and copper water nanofluids with mixed convection and nonlinear thermal radiation, Int. J. Heat Mass Transf. 102 (2016) 723–732.

[29] **M. Imtiaz, T. Hayat, A. Alsaedi,** Mixed convection flow of Casson nanofluid over a stretching cylinder with convective boundary conditions, Adv. Powd. Tech. 27 (5) (2016) 2245–2256.

[30] **M. Imtiaz, T. Hayat, A. Alsaedi,** Flow of magneto-nanofluid by a radiative exponentially stretching surface with dissipation effect, Adv. Powd. Tech. 27 (5) (2016) 2214–2222.

[31] **T. Hayat, S. Qayyum, A. Alsaedi, A. Shafiq,** Inclined magnetic field and heat source/sink aspects in flow of nanofluid with nonlinear thermal radiation, Int. J. Heat Mass Transf. 103 (2016) 99–107.

[32] **T. Hayat, M. Imtiaz, A. Alsaedi,** Melting heat transfer in the MHD flow of Cu–water nanofluid with viscous dissipation and Joule heating, Adv. Powd. Tech. 27(4) (2016) 1301–1308.

[33] **M. Sajid, T. Javed, T. Hayat,** MHD rotating flow of a viscous fluid over a shrinking surface, Nonlin. Dyn. 51 (1) (2008) 259–265.

[34] **K.L. Hsiao,** Stagnation electrical MHD nanofluid mixed convection with slip boundary on a stretching sheet, Appl. Therm. Eng. 98 (2016) 850–861.

[35] **K.L. Hsiao,** Nanofluid flow with multimedia physical features for conjugate mixed convection and radiation, Comp. Fluids. 104 (2014) 1–8.

[36] **K.L. Hsiao,** To promote radiation electrical MHD activation energy thermal extrusion manufacturing system efficiency by using carreau nanofluid with parameters control method, Energy. 130 (2017) 486–499.

[37] **K.L. Hsiao,** Micropolar nanofluid flow with MHD and viscous dissipation effects towards a stretching sheet with multimedia feature, Int. J. Heat Mass Transf. 112 (2017) 983–990.

[38] **K.L. Hsiao,** Combined electrical MHD heat transfer thermal extrusion system using Maxwell fluid with radiative and viscous dissipation effects, Appl. Therm. Eng. 112 (2017) 1281–1288.

[39] **A.K. Pandey, M. Kumar,** Boundary layer flow and heat transfer analysis on Cu–water nanofluid flow over a stretching cylinder with slip, Alexandria Eng. J. (2017) (in press) https://doi.org/10.1016/j.aej.2017.01.017.

[40] **T. Hayat, S. Qayyum, A. Alsaedi, S.A. Shehzad,** Nonlinear thermal radiation aspects in stagnation point flow of tangent hyperbolic nanofluid with double diffusive convection, J. Molec. Liq. 223 (2016) 969–978.

[41] **M. Mustafa, S. Hina, T. Hayat, A. Alsaedi,** Influence of wall properties on the peristaltic flow of a nanofluid: analytic and numerical solutions, Int. J. Heat Mass Transf. 55 (17) (2012) 4871–4877.

[42] **M.A. Chaudhary, J.H. Merkin,** A simple isothermal model for homogeneous-heterogeneous reactions in boundary-layer flow. I. Equal diffusivities, Fluid Dyn. Res. 16 (6) (1995) 311–333.

[43] **M.I. Khan, T. Hayat, M.I. Khan, A. Alsaedi,** A modified homogeneous-heterogeneous reactions for MHD stagnation flow with viscous dissipation and Joule heating, Int. J. Heat Mass Transf. 113 (2017) 310–317.

[44] **T. Hayat, M. Rashid, M. Imtiaz, A. Alsaedi,** Nanofluid flow due to rotating disk with variable thickness and homogeneous-heterogeneous reactions, Int. J. Heat Mass Transf. 113 (2017) 96–105.

[45] **A. Tanveer, T. Hayat, A. Alsaedi, B. Ahmad,** Mixed convective peristaltic flow of Sisko fluid in curved channel with homogeneous-heterogeneous reaction effects, J. Molec. Liq. 233 (2017) 131–138.

[46] **T. Hayat, Z. Hussain, A. Alsaedi, B. Ahmad,** Heterogeneous-homogeneous reactions and melting heat transfer effects in flow with carbon nanotubes, J. Molec. Liq. 220 (2016) 200–207.

[47] **M. Farooq, A. Anjum, T. Hayat, A. Alsaedi,** Melting heat transfer in the flow over a variable thicked Riga plate with homogeneous-heterogeneous reactions, J. Molec. Liq. 224 (2016) 1341–1347.

[48] **T. Hayat, Z. Hussain, M. Farooq, A. Alsaedi,** Effects of homogeneous and heterogeneous reactions and melting heat in the viscoelastic fluid flow, J. Molec. Liq. 215 (2016) 749–755.

[49] **T. Hayat, M.I. Khan, M. Farooq, T. Yasmeen, A. Alsaedi,** Stagnation point flow with Cattaneo – Christov heat flux and homogeneous-heterogeneous reactions, J. Molec. Liq. 220 (2016) 49–55.

[50] **T. Hayat, M. Imtiaz, A. Alsaedi, F. Alzahrani,** Effects of homogeneous–heterogeneous reactions in flow of magnetite-Fe_3O_4 nanoparticles by a rotating disk, J. Molec. Liq. 216 (2016) 845–855.

Received 09.03.2017, accepted 10.10.2017.

THE AUTHORS

PANDEY Alok Kumar
Roorkee Institute of Technology
8th km Dehradun Road, Puhana, Roorkee, Uttarakhand, 247667, India
mr.alokpandey1@gmail.com

KUMAR Manoj
G.B. Pant University of Agriculture and Technology
District-Udham Singh Nagar, Pantnagar, Uttarakhand, 263153, India
mnj_kumar2004@yahoo.com

СПИСОК ЛИТЕРАТУРЫ

1. **Choi S.U.S.** Enhancing thermal conductivity of fluids with nanoparticles // ASME-Publications-Fed. 1995. Vol. 231. Pp. 99–106.

2. **Ariel P.D.** Hiemenz flow in hydromagnetics // Acta Mech. 1994. Vol. 103. Vol. 1–4. Pp. 31–43.

3. **Ganapathirao M., Ravindran R.** Nonuniform slot suction/injection into mixed convective MHD flow over a vertical wedge with chemical reaction // Procedia Eng. 2015. Vol. 127. Pp. 1102–1109.

4. **Rahman M.M., Al-Lawatia M.A., Eltayeb I.A., Al-Salti N.** Hydromagnetic slip flow of water based nanofluids past a wedge with convective surface in the presence of heat generation (or) absorption // Int. J. Therm. Sci. 2012. Vol. 57. Pp. 172–182.

5. **Srinivasacharya D., Mendu U., Venumadhav K.** MHD boundary layer flow of a nanofluid past a wedge // Procedia Eng. 2015. Vol. 127. Pp. 1064–1070.

6. **Rahman A.M., Alam M.S., Alim M.A., Chowdhury M.K.** Unsteady MHD forced convective heat and mass transfer flow along a wedge with variable electric conductivity and thermophoresis // Procedia Eng. 2013. Vol. 56. Pp. 531–537.

7. **Yacob N.A., Ishak A., Pop I.** Falkner – Skan problem for a static or moving wedge in nanofluids // Int. J. Therm. Sci. 2011. Vol. 50. No. 2. Pp. 133–139.

8. **Nagendramma V., Sreelakshmi K., Sarojamma G.** MHD heat and mass transfer flow over a stretching wedge with convective boundary condition and thermophoresis // Procedia Eng. 2015. Vol. 127. Pp. 963–969.

9. **Kandasamy R., Muhaimin I., Rosmila A.K.** The performance evaluation of unsteady MHD non-Darcy nanofluid flow over a porous wedge due to renewable (solar) energy // Renew. Energy. 2014. Vol. 64. Pp. 1–9.

10. **Pandey A.K., Kumar M.** Effect of viscous dissipation and suction/injection on MHD nanofluid flow over a wedge with porous medium and slip // Alexandria Eng. J. 2016. Vol. 55. No. 4. Pp. 3115–3123.

11. **Pandey A.K., Kumar M.** Natural convection and thermal radiation influence on nanofluid flow over a stretching cylinder in a porous medium with viscous dissipation // Alexandria Eng. J. 2017. Vol. 56. No. 1. Pp. 55–62.

12. **Khanafer K., Vafai K., Lightstone M.** Buoyancy-driven heat transfer enhancement in a two-dimensional enclosure utilizing nanofluids // Int. J. Heat Mass Transf. 2003. Vol. 46. No. 19. Pp. 3639–3653.

13. **Buongiorno J.** Convective transport in nanofluids // ASME J. Heat Transf. 2006. Vol. 128. No. 3. Pp. 240–250.

14. **Tiwari R.K., Das M.K.** Heat transfer augmentation in two-sided lid-driven differentially heated square cavity utilizing nanofluids // Int. J. Heat Mass Transf. 2007. Vol. 50. No. 9. Pp. 2002–2018.

15. **Sheikholeslami M., Abelman S.** Two-phase simulation of nanofluid flow and heat transfer in an annulus in the presence of an axial magnetic field // IEEE Trans. Nanot. 2015. Vol. 14. No. 3. Pp. 561–569.

16. **Sheikholeslami M., Ganji D.D., Rashidi M.M.** Magnetic field effect on unsteady nanofluid flow and heat transfer using Buongiorno model // J. Magn. Magn. Mater. 2016. Vol. 416. Pp. 164–173.

17. **Hayat T., Waqas M., Shehzad S.A., Alsaedi A.** A model of solar radiation and Joule heating in magnetohydrodynamic (MHD) convective flow of thixotropic nanofluid // J. Mol. Liq. 2016. Vol. 215. Pp. 704–710.

18. **Ziaei-Rad M., Saeedan M., Afshari E.** Simulation and prediction of MHD dissipative nanofluid flow on a permeable stretching surface using artificial neural network // Appl. Therm. Eng. 2016. Vol. 99. Pp. 373–382.

19. **Sheikholeslami M., Hayat T., Alsaedi A.** MHD free convection of Al_2O_3–water nanofluid considering thermal radiation: a numerical study // Int. J. Heat Mass Transf. 2016. Vol. 96. Pp. 513–524.

20. **Zhang C., Zheng L., Zhang X., Chen G.** MHD flow and radiation heat transfer of nanofluids

in porous media with variable surface heat flux and chemical reaction // Appl. Math. Modell. 2015. Vol. 39. No. 1. Pp. 165–181.

21. **Das K., Duari P.R., Kundu P.K.** Numerical simulation of nanofluid flow with convective boundary condition // J. Egypt. Math. Soc. 2015. Vol. 23. No. 2. Pp. 435–439.

22. **Pal D., Mandal G.** Hydromagnetic convective-radiative boundary layer flow of nanofluids induced by a nonlinear vertical stretching/shrinking sheet with viscous – Ohmic dissipation // Powder Technol. 2015. Vol. 279. Pp. 61–74.

23. **Hayat T., Ashraf M.B., Shehzad S.A., Alsaedi A.** Mixed convection flow of Casson nanofluid over a stretching sheet with convectively heated chemical reaction and heat source/sink // J. Appl. Fluid Mech. 2015. Vol. 8. No. 4. Pp. 803–813.

24. **Hayat T., Khan M.I., Waqas M., Yasmeen T., Alsaedi A.** Viscous dissipation effect in flow of magneto-nanofluid with variable properties // J. Mol. Liq. 2016. Vol. 222. Pp. 47–54.

25. **Hayat T., Khan M.I., Waqas M., Alsaedi A., Yasmeen T.** Diffusion of chemically reactive species in third grade flow over an exponentially stretching sheet considering magnetic field effects // Chinese J. Chem. Eng. 2016. Vol. 25. No. 3. Pp. 257–263.

26. **Upreti H., Pandey A.K., Kumar M.** MHD flow of Ag – water nanofluid over a flat porous plate with viscous – Ohmic dissipation, suction/injection and heat generation/absorption // Alexandria Eng. J. 2017. (in press) https://doi.org/10.1016/j.aej.2017.03.018.

27. **Hayat T., Shafiq A., Imtiaz M., Alsaedi A.** Impact of melting phenomenon in the Falkner – Skan wedge flow of second grade nanofluid: A revised model // J. Molec. Liq. 2016. Vol. 215. Pp. 664–670.

28. **Hayat T., Qayyum S., Imtiaz M., Alsaedi A.** Comparative study of silver and copper water nanofluids with mixed convection and nonlinear thermal radiation // Int. J. Heat Mass Transf. 2016. Vol. 102. Pp. 723–732.

29. **Imtiaz M., Hayat T., Alsaedi A.** Mixed convection flow of Casson nanofluid over a stretching cylinder with convective boundary conditions // Adv. Powd. Tech. 2016. Vol. 27. No. 5. Pp. 2245–2256.

30. **Imtiaz M., Hayat T., Alsaedi A.** Flow of magneto nanofluid by a radiative exponentially stretching surface with dissipation effect // Adv. Powd. Tech. 2016. Vol. 27. No. 5. Pp. 2214–2222.

31. **Hayat T., Qayyum S., Alsaedi A., Shafiq A.** Inclined magnetic field and heat source/sink aspects in flow of nanofluid with nonlinear thermal radiation // Int. J. Heat Mass Transf. 2016. Vol. 103. Pp. 99–107.

32. **Hayat T., Imtiaz M., Alsaedi A.** Melting heat transfer in the MHD flow of Cu–water nanofluid with viscous dissipation and Joule heating // Adv. Powd. Tech. 2016. Vol. 27. No. 4. Pp. 1301–1308.

33. **Sajid M., Javed T., Hayat T.** MHD rotating flow of a viscous fluid over a shrinking surface // Nonlin. Dyn. 2008. Vol. 51. No. 1. Pp. 259–265.

34. **Hsiao K.L.** Stagnation electrical MHD nanofluid mixed convection with slip boundary on a stretching sheet // Appl. Therm. Eng. 2016. Vol. 98. Pp. 850–861.

35. **Hsiao K.L.** Nanofluid flow with multimedia physical features for conjugate mixed convection and radiation // Comp. Fluids. 2014. Vol. 104. Pp. 1–8.

36. **Hsiao K.L.** To promote radiation electrical MHD activation energy thermal extrusion manufacturing system efficiency by using carreau nanofluid with parameters control method // Energy. 2017. Vol. 130. Pp. 486–499.

37. **Hsiao K.L.** Micropolar nanofluid flow with MHD and viscous dissipation effects towards a stretching sheet with multimedia feature // Int. J. Heat Mass Transf. 2017. Vol. 112. Pp. 983–990.

38. **Hsiao K.L.** Combined electrical MHD heat transfer thermal extrusion system using Maxwell fluid with radiative and viscous dissipation effects // Appl. Therm. Eng. 2017. Vol. 112. Pp. 1281–1288.

39. **Pandey A.K., Kumar M.** Boundary layer flow and heat transfer analysis on Cu–water nanofluid flow over a stretching cylinder with slip // Alexandria Eng. J. 2017. (in press) https://doi.org/10.1016/j.aej.2017.01.017.

40. **Hayat T., Qayyum S., Alsaedi A., Shehzad S.A.** Nonlinear thermal radiation aspects in stagnation point flow of tangent hyperbolic nanofluid with double diffusive convection // J. Molec. Liq. 2016. Vol. 223. Pp. 969–978.

41. **Mustafa M., Hina S., Hayat T., Alsaedi A.** Influence of wall properties on the peristaltic flow of a nanofluid: analytic and numerical solutions // Int. J. Heat Mass Transf. 2012. Vol. 55. No. 17–18. Pp. 4871–4877.

42. **Chaudhary M.A., Merkin J.H.** A simple isothermal model for homogeneous-heterogeneous reactions in boundary-layer flow. I. Equal diffusivities // Fluid Dyn. Res. 1995. Vol. 16. No. 6. Pp. 311–333.

43. **Khan M.I., Hayat T., Khan M.I., Alsaedi A.** A modified homogeneous-heterogeneous reactions for MHD stagnation flow with viscous dissipation and Joule heating // Int. J. Heat Mass Transf. 2017. Vol. 113. Pp. 310–317.

44. **Hayat T., Rashid M., Imtiaz M., Alsaedi A.** Nanofluid flow due to rotating disk with variable thickness and homogeneous-heterogeneous reac-

tions // Int. J. Heat Mass Transf. 2017.Vol. 113. Pp. 96–105.

45. **Tanveer A., Hayat T., Alsaedi A., Ahmad B.** Mixed convective peristaltic flow of Sisko fluid in curved channel with homogeneous-heterogeneous reaction effects // J. Molec. Liq. 2017. Vol. 233. Pp. 131–138.

46. **Hayat T., Hussain Z., Alsaedi A., Ahmad B.** Heterogeneous-homogeneous reactions and melting heat transfer effects in flow with carbon nanotubes // J. Molec. Liq. 2016. Vol. 220. Pp. 200–207.

47. **Farooq M., Anjum A., Hayat T., Alsaedi A.** Melting heat transfer in the flow over a variable thicked Riga plate with homogeneous-heterogeneous reactions // J. Molec. Liq. 2016. Vol. 224. Pp. 1341–1347.

48. **Hayat T., Hussain Z., Farooq M., Alsaedi A.** Effects of homogeneous and heterogeneous reactions and melting heat in the viscoelastic fluid flow // J. Molec. Liq. 2016. Vol. 215. Pp. 749–755.

49. **Hayat T., Khan M.I., Farooq M., Yasmeen T., Alsaedi A.** Stagnation point flow with Cattaneo – Christov heat flux and homogeneous-heterogeneous reactions // J. Molec. Liq. 2016. Vol. 220. Pp. 49–55.

50. **Hayat T., Imtiaz M., Alsaedi A., Alzahrani F.** Effects of homogeneous–heterogeneous reactions in flow of magnetite-Fe_3O_4 nanoparticles by a rotating disk // J. Molec. Liq. 2016. Vol. 216. Pp. 845–855.

Статья поступила в редакцию 09.03.2017, принята к публикации 10.10.2017.

СВЕДЕНИЯ ОБ АВТОРАХ

ПАНДИ Алок Кумар – *сотрудник кафедры математики Индийского технологического института Рурки, г. Рурки, Индия.*

8th km Dehradun Road, Puhana, Roorkee, Uttarakhand 247667, India
mr.alokpandey1@gmail.com

КУМАР Манодж – *сотрудник Колледжа фундаментальных и гуманитарных наук Университета сельского хозяйства и технологии им. Говинда Балабаха Панта, г. Пантнагар, Индия.*

District Udham Singh Nagar, Pantnagar, Uttarakhand 263153, India
mnj_kumar2004@yahoo.com

© Санкт-Петербургский политехнический университет Петра Великого, 2017